Effects of modifier additions on the thermal properties, chemical durability, oxidation state and structure of iron phosphate glasses

P.A. Bingham[a,*], R.J. Hand[a], O.M. Hannant[a], S.D. Forder[b], S.H. Kilcoyne[c]

[a] Immobilisation Science Laboratory, Department of Engineering Materials, University of Sheffield, Mappin Street, Sheffield S1 3JD, UK

[b] Materials and Engineering Research Institute, Sheffield Hallam University, Howard Street, Sheffield S1 1WB, UK

[c] School of Computing, Science and Engineering, University of Salford, Salford, Greater Manchester M5 4WT, UK

Received 17 June 2008; revised 13 March 2009; Available online 17 June 2009.

Abstract

Modified iron phosphate glasses have been prepared with nominal molar compositions $[(1-x)\cdot(0.6P_2O_5-0.4Fe_2O_3)]\cdot xR_ySO_4$, where $x = 0–0.5$ in increments of 0.1 and R = Li, Na, K, Mg, Ca, Ba, or Pb and $y = 1$ or 2. In most cases the vast majority or all of the sulfate volatalizes and quarternary $P_2O_5–Fe_2O_3–FeO–R_yO_z$ glasses or partially crystalline materials are formed. Here we have characterized the structure, thermal properties, chemical durability and redox state of these materials. Raman spectroscopy indicates that increasing modifier oxide additions result in depolymerization of the phosphate network such that the average value of i, the number of bridging oxygens per $–(PO_4)–$ tetrahedron, and expressed as Q^i, decreases. Differences have been observed between the structural effects of different modifier types but these are secondary to the amount of modifier added. Alkali additions have little effect on density; slightly increasing T_g and T_d; increasing α and T_{liq}; and promoting bulk crystallization at temperatures of 600–700 °C. Additions of divalent cations increase density, α, T_g, T_d, T_{liq} and promote bulk crystallization at temperatures of 700–800 °C. Overall the addition of divalent cations has a less deleterious effect on glass stability than alkali additions. ^{57}Fe Mössbauer spectroscopy confirms that iron is present as Fe^{2+} and Fe^{3+} ions which primarily occupy distorted octahedral sites. This is consistent with accepted structural models for iron phosphate glasses. The iron redox ratio, $Fe^{2+}/\Sigma Fe$, has a value of 0.13–0.29 for the glasses studied. The base glass exhibits a very low aqueous leach rate when measured by Product Consistency Test B, a standard durability test for nuclear waste glasses. The addition of high quantities of alkali oxide (30–40 mol% R_2O) to the base glass increases leach rates, but only to levels comparable with those measured for a commercial soda-lime-silica glass and for a surrogate nuclear waste-loaded borosilicate glass. Divalent cation additions decrease aqueous leach rates and large additions (30–50 mol% RO) provide exceptionally low leach rates that are 2–3 orders of magnitude lower than have been measured for the surrogate waste-loaded borosilicate glass. The $P_2O_5–Fe_2O_3–FeO–BaO$ glasses reported here show particular promise as they are ultra-durable, thermally stable, low-melting glasses with a large glass-forming compositional range.

PACS: 61.43.Fs; 65.60.+a; 76.80.+y; 63.50.–x

Keywords: Chemical durability; Composition; Nuclear and chemical wastes; Optical properties; Raman spectroscopy; Oxide glasses; Phosphates

1. Introduction

Alkali borosilicate glasses are currently the global material of choice for the safe immobilization of high-level radioactive waste (HLW) which is highly radioactive and heat-generating. Silicate glasses are also the obvious host matrix for the vitrification of toxic incinerator ashes given that these wastes are usually rich in SiO_2. Phosphate glasses by comparison have few applications; however, they have received substantial attention over the past 40–50 years as possible host materials for the immobilization of certain specific radioactive wastes [1], [2], [3], [4] and [5]. Some Russian HLW has been immobilized in sodium aluminophosphate glasses at the Mayak facility in Ozersk [4] and [5]. The formation of

phosphate glasses by vitrification of phosphate-rich sludges from the fabricated metal products industry has also recently been investigated [6] and [7].

Sodium aluminophosphate glasses can, in some cases, provide advantages over alkali borosilicate glasses. These advantages include lower melting temperatures and higher waste loading capacities. However, phosphate glasses are generally more corrosive towards refractory melter linings and have relatively low thermal stabilities [2] and [3] although recent work has demonstrated that small additions of B_2O_3 to sodium aluminophosphate [8] and SiO_2, Al_2O_3 or B_2O_3 to iron phosphate [9] and [10]glass compositions can substantially improve their thermal stability. Thermal stability is important because the incorporation of heat-generating wastes and/or the presence of high temperatures in underground repositories can cause glasses with low thermal stabilities to crystallize, which can in turn lead to volume changes and may impair the chemical durability and mechanical performance of the waste form. Published research into phosphate glasses for waste immobilization focussed largely on lead–iron phosphate glasses during the 1980s [1], [2] and [3]. However, concerns remain regarding lead–iron phosphate glasses in terms of their corrosivity during melting, thermal stability and their chemical durability [3].

Iron phosphate glasses have been studied for their potential waste immobilization applications since the mid-1990s [2]. A substantial proportion of this research has dealt with formulations based on the ternary P_2O_5–Fe_2O_3–FeO system, and particularly around the familiar $60P_2O_5$–$40Fe_2O_3$ (mol%) composition and derivatives there of. Due to the often complex chemical nature of waste-loaded glasses it can be useful to simplify their compositions in order to study individual components and their effects on properties and structure. These data can provide useful information and around which specific experiments involving actual radioactive wastes or simulants may be based. Several published studies deal with P_2O_5–Fe_2O_3–FeO–R_xO_y glasses, for which R = Na [11], [12], [13], [14] , [15], [16], [17], [18], [19], [20] and [21], K [19] and [22], Cs [16], [17], [23], [24] and [25], Ca [16], [26] and [27], Sr [17], [24] and [28], Ba [29], [30] and [31], Zn [20], [32] and [33], Pb [1], [2] and [3], Al [10], [13] and [21], B [9] and [10] and Si [10]. Despite this apparent depth of information there exists little published data which allows direct comparisons to be made between the effects of different types and different contents of modifier cations upon the properties of the resulting materials. Nor have the effects of components less commonly associated with ‘legacy’ nuclear wastes or with HLW been researched in any great depth. Documented glass formation, structure and property information for these systems is therefore far from comprehensive.

Recently we have studied glass formation and the solubility of SO_3 in $60P_2O_5$–$40Fe_2O_3$ (mol%) glasses to which have been added oxides of monovalent (Li, Na, and K) and divalent (Mg, Ca, Ba, and Pb) cations. These oxides were supplied to the glasses through the use of sulfate batch materials. This has allowed assessments of the glass formation region (for glasses cooled in air on a 200 g scale) and sulfate solubility [34] and some effects of batch sulfate on iron redox [35] in these materials. With few exceptions, low levels (<0.5 mol%) of sulfate remained in the resulting glassy or crystalline materials. Consequently these materials may be essentially regarded as occupying the P_2O_5–Fe_2O_3–FeO–R_xO_y system. The research described in the present paper further describes our ongoing studies into the effects of doping iron phosphate glasses with R_xO_y, where R = selected R^+, R^{2+}, R^{3+} and R^{4+} cations, and their effects upon properties and structure. Primarily our motivation is the development and understanding of new glasses with potential applications in radioactive or toxic waste immobilization; however, the information that we have generated may also prove useful to those researching the use of iron phosphate glasses in other applications.

2. Experimental procedures

Glasses have been prepared from analytical grade >99 % purity $NH_4H_2PO_4$, Fe_2O_3, Li_2SO_4, Na_2SO_4, Na_2CO_3, K_2SO_4, $MgSO_4$, $CaSO_4$, $BaSO_4$ and [PbO + $(NH_4)_2SO_4$]. Batches to produce 200 g of glass with nominal molar composition $[(1-x)\cdot(0.6P_2O_5–0.4Fe_2O_3)]\cdot xR_2SO_4$, where x = 0–0.5, were placed in mullite ($3Al_2O_3\cdot2SiO_2$) crucibles and heated overnight to 1030 °C. Crucibles were then transferred to a furnace at 1150 °C and held at this temperature for 1 h. Melts were stirred at ~60 rpm at 1150 °C for a further 2 h using Al_2O_3 stirrers. Samples were finally poured into preheated steel molds, held at 450–475 °C for 1 h to relieve internal stresses, and cooled to room temperature at 1 °C/min. A glass of nominal composition $60P_2O_5$–$40Fe_2O_3$ (mol%), named PFe1M, has been used as the baseline glass. Sample name nomenclature is as follows: modifier added, and oxide quantity in mol%. Hence sample Ba30S was batched to produce a sample containing 30 mol% $BaSO_4$ such that nominal molar composition was $42P_2O_5$–$28Fe_2O_3$–$30BaSO_4$. Given that most or all of the sulfate volatilized, presumably as (SO_2 + $1/2O_2$), the actual molar composition of the resulting glass is

close to $42P_2O_5$–$28Fe_2O_3$–30BaO. Material bulk compositions have been analyzed previously [34] and [35] and confirm this assertion, although some SO_3 and SiO_2 and Al_2O_3 arising from crucible corrosion have been measured in most samples. Nevertheless the (generally) low levels of contamination of the samples described in this paper means that they may be considered to occupy the P_2O_5–Fe_2O_3–FeO–R_xO_y system. Nominal and analyzed compositions are included again here for completeness. One sample, Na20, was prepared using Na_2CO_3 rather than Na_2SO_4, in order to assess any effects upon final glass redox of using sulfate raw materials. Its final composition, shown in Table 1, is very close to that of its companion glass, Na20S.

Table 1. Nominal and analyzed composition and measured properties for $[(1-x)\cdot(0.6P_2O_5–0.4Fe_2O_3)]\cdot xR_2O$ glasses.

Sample name	**PFe1M**	**Li10S**	**Li20S**	**Na10S**	**Na20S**	**Na20**	**Na30S**	**Na40S**	**K10S**	**K20S**	**K30S**	**K40S**
P_2O_5 mol% (analyzed)	60.0 (60.9)	49.08 (52.8)	40.00 (47.8)	49.08 (53.4)	40.00 (44.8)	48.0 (44.6)	32.30 (37.1)	28.57 (30.8)	49.08 (53.4)	40.00 (45.8)	32.30 (40.0)	25.71 (32.6)
Fe_2O_3 mol % (analyzed)	40.0 (38.0)	32.72 (32.3)	26.66 (28.8)	32.72 (32.2)	26.66 (27.1)	32.0 (27.6)	21.54 (23.3)	17.14 (18.8)	32.72 (33.3)	26.66 (28.3)	21.54 (24.9)	17.14 (22.2)
SiO_2 mol% (analyzed)	0 (0.5)	0 (1.1)	0 (2.3)	0 (0.4)	0 (3.2)	0 (3.1)	0 (4.8)	0 (7.2)	0 (0.8)	0 (3.6)	0 (2.8)	0 (4.2)
Al_2O_3 mol% (analyzed)	0 (0.6)	0 (1.1)	0 (1.5)	0 (0.7)	0 (2.4)	0 (2.6)	0 (4.4)	0 (5.5)	0 (0.8)	0 (2.8)	0 (2.6)	0 (2.5)
Li_2O mol% (analyzed)	0 (n/m[a])	9.10 (10.3)	16.67 (18.0)	0 (n/m[a])	0 (n/m[a])	0 (n/m[a])	0 (n/m[a])	0 (n/m[a])	0 (n/m[a])	0 (n/m[a])	0 (n/m[a])	0 (n/m[a])
Na_2O mol% (analyzed)	0 (0)	0 (1.9)	0 (1.3)	9.10 (12.9)	16.67 (22.1)	20.0 (21.5)	23.08 (29.7)	28.57 (36.9)	0 (1.9)	0 (1.2)	0 (1.8)	0 (1.7)
K_2O mol% (analyzed)	0 (0)	0 (0.3)	0 (0.2)	0 (0.2)	0 (0.3)	0 (0.6)	0 (0.6)	0 (0.5)	9.10 (9.7)	16.67 (18.2)	23.08 (27.6)	28.57 (35.6)
SO_3 equiv. mol% (analyzed)	0 (n/m[a])	9.10 (0.130)	16.67 (0.068)	9.10 (0.038)	16.67 (0.055)	0 (0)	23.08 (0.058)	28.57 (0.400)	9.10 (0.070)	16.67 (0.108)	23.08 (0.343)	28.57 (1.2)
Phase/s identified	Am[b]	Am[b]	LiFe(P_2O_7) / $Fe_7(PO_4)_6$	Am[b]	Am[b]	n/m[a]	Am[b]	$Na_3Fe_2(PO_4)_3$	Am[b]	Am[b]	Am[b]	Unident. phase/s
$\rho \pm 0.005$/g cm^{-3}	2.988	3.079	3.085	3.096	3.113	n/m[a]	3.096	3.009	3.031	2.964	2.977	2.897
$V_m \pm 1$ (cm^3 mol^{-1})	49.59	43.18	39.93	44.05	40.24	n/m[a]	37.55	35.67	46.40	44.94	43.09	42.23
($\alpha_{50–300} \times 10^{-7}$)±2/ ℃	68	92	105	90	120	n/m[a]	136	155	93	109	145	n/m[a]
Dilat. mid-point T_g±2/ ℃	505	485	487	503	491	n/m[a]	497	482	519	526	506	n/m[a]
Dilat. $T_d \pm$ 2/ ℃	534	501	506	527	513	n/m[a]	513	503	543	552	532	n/m[a]
DTA mid-point $T_g \pm$ 2/ ℃	500	508	n/m[a]	518	526	n/m[a]	525	n/m[a]	529	537	532	n/m[a]
DTA onset $T_r \pm$ 2/ ℃	612	588	n/m[a]	638	642	n/m[a]	555	n/m[a]	642	657	588	n/m[a]
DTA ($T_r - T_g$) ± 4/ ℃	128	98	n/m[a]	127	120	n/m[a]	55	n/m[a]	121	132	67	n/m[a]
DTA $T_{liq} \pm$ 2/℃	950	992	n/m[a]	1014	1022	n/m[a]	920	n/m[a]	1031	1065	937	n/m[a]
Mössbauer $Fe^{2+}/\Sigma Fe \pm$ 0.02	0.133	0.212	n/m[a]	0.215	0.271	0.290	0.209	n/m[a]	0.214	0.235	0.163	n/m[a]

Sample name	PFe1M	Li10S	Li20S	Na10S	Na20S	Na20	Na30S	Na40S	K10S	K20S	K30S	K40S
Mössbauer CS (Fe^{3+}) ± 0.02	0.37	0.38	n/m[a]	0.38	0.39	0.38	0.39	n/m[a]	0.38	0.38	0.38	n/m[a]
Mössbauer QS (Fe^{3+}) ± 0.02	0.89	0.90	n/m[a]	0.90	0.90	0.87	0.86	n/m[a]	0.90	0.88	0.82	n/m[a]
Mössbauer CS (Fe^{2+}) ± 0.02	1.25	1.31	n/m[a]	1.28	1.27	1.26	1.25	n/m[a]	1.28	1.27	1.26	n/m[a]
Mössbauer QS (Fe^{2+}) ± 0.02	2.13	2.11	n/m[a]	2.02	2.02	2.08	2.00	n/m[a]	2.02	1.93	1.89	n/m[a]

[a] n/m, Not measured.

[b] Am, amorphous.

Material bulk compositions have been analyzed using a Link energy-dispersive X-ray spectroscopy (EDS) unit fitted to a Philips 500 scanning electron microscope. The analyzed compositions shown in Table 1 and Table 2 are averages from three separate measurements. Estimated errors associated with each measurement are as follows: (i) major components (>10 mol%) error ± 1 mol%, (ii) intermediate components (1–10 mol%) error ± 0.5 mol%, (iii) minor components (<1 mol%) error ± 0.1 mol%. Lithium contents have been measured, for those samples containing lithium batch additions (glasses Li10S and Li20S), by inductively-coupled plasma-optical emission spectroscopy (ICP-OES). The accuracy of this technique is estimated to be ±0.1 mol% Li_2O. Sulfur contents were analyzed both by EDS and using a Leco induction furnace combustion analyzer and a combustion/infrared analyzer in order to gain greater accuracy. For analytical purposes the sulfur contents have been expressed in Table 1 and Table 2as sulfate (SO_3). Sulfur analyzes carry estimated accuracies of ±0.01 mol% SO_3. Combined SEM and visual analyzes confirm that there is no evidence of phase separation in the sulfate-containing glasses studied here. It is known that iron occurs as Fe^{2+} (FeO) and Fe^{3+} (Fe_2O_3) in iron phosphate glasses but iron contents are presented here as equivalent Fe_2O_3 for simplicity.

Two glasses have also been used as comparators for the chemical durability studies. The first, SLS, is a commercial soda-lime-silica container glass and the second, a surrogate waste-loaded UK HLW borosilicate glass. The HLW glass composition and preparation method has been described in [36]. The SLS glass composition has been analyzed using the same EDS method and equipment used to analyze the iron phosphate glasses [34] and [35], and has the following analyzed composition (mol%): 71.3SiO_2, 12.2CaO, 13.1Na_2O, 2.3MgO, 0.6Al_2O_3, 0.2K_2O, and 0.2SO_3.

Densities have been measured by the Archimedes method using distilled water as the suspension medium. Archimedes densities are calculated using $\text{Density}=[W_A/(W_A-W_w)]\times\delta_w$, (1) where W_A = weight in air, W_W = weight in water and δ_w = temperature correction. Molar volumes have been calculated using measured densities and analyzed compositions [34] and [35].

Differential thermal analysis (DTA) has been performed using a Perkin–Elmer DTA 7 instrument. Powdered 25 mg samples of particle size <75 μm are placed in recrystallized Al_2O_3 sample cups and heated at 10 °C/min from 20 °C to 1200 °C.

Dilatometric measurements have been made between room temperature and 10–20 °C above the dilatometric softening point, T_d, at a heating rate of 10 °C/min, using a Netzsch DIL402C dilatometer. Samples are ~20 mm in length, approximately circular in cross section and with ~3 mm radius. Repeat measurements have confirmed that measurements obtained from this equipment using a heating rate of 10 °C/min are acceptably accurate and reproducible within the error range specified. The linear coefficient of thermal expansion from 50–300 ° (α_{50-300}), mid-point glass transition temperature T_g and dilatometric softening point, T_d, have all been determined using the dilatometer's software package. We note that for some samples the value of T_g as measured by DTA and dilatometry differ by an amount greater than the combined estimated errors of measurement. The origin of these differences is not clear and may be related to differences in sample preparation, given that DTA requires a powdered sample and dilatometry uses a

monolithic sample. Heating rates for the two techniques were nominally the same, but small differences may have occurred which would, in particular, affect the measured values of T_g and T_d. The trends in parameters observed as a function of modifier type and content remain approximately the same between the two techniques, therefore both data sets have been included here for completeness. However, DTA results are more widely used for T_g determination.

Room temperature Mössbauer spectra have been collected relative to α-Fe over the velocity range ±5 mm s^{-1} using a constant acceleration spectrometer with a 25 mCi source of ^{57}Co in Rh. Eight broadened Lorentzian paramagnetic doublets have been fitted to each spectrum, four for Fe^{2+} and four for Fe^{3+}, using the Recoil analysis software package [37]. Extracted center shift (CS), quadrupole splitting (QS) and line width (LW) parameters are weighted averages based on doublet areas. Multiple Lorentzian doublets have been widely used to fit Mössbauer spectra of iron phosphate glasses [7], [9], [10], [13], [17], [25] and [32]. The redox ratio, $Fe^{2+}/\Sigma Fe$, is based on fitted peak areas, corrected for the recoil-free fraction ratio $f(Fe^{3+})/f(Fe^{2+}) \approx 1.30$ in phosphate glasses at room temperature, as we have discussed previously [7] and [9].

X-ray diffraction (XRD) has been carried out using a Philips PW1730/10 goniometer with CuKα radiation. Spectra have been recorded from 10 to 60° 2θ at scanning rates between 0.1 and 0.4° 2θ/min.

Laser Raman spectroscopy has been carried out on flat, polished samples using 514.5 nm radiation and a Renishaw inVia spectrometer coupled with an optical microscope. Spectra are measured at 20× magnification from 0 to 1500 cm^{-1} and recorded by a computer.

Chemical durability measurements have been conducted according to Product Consistency Test B (PCT–B) [38], using 3 g of sample glass with size fraction 75–150 μm in 30 g distilled water leachant solution. Tests have been carried out in duplicate at 90 °C for 7 days. Leachate solutions are then filtered and analyzed by inductively-coupled plasma optical emission spectroscopy (ICP-OES); correction of data by subtracting the normalized analysis for accompanying blank solutions is then made.

3. Results

Analyzed glass compositions and measured properties are shown in Table 1 and Table 2. Figs. 1(a) and (b) illustrate density and molar volume, respectively, as functions of nominal modifier oxide content. The experimental errors are smaller than the data points shown. XRD analysis has confirmed that the majority of samples are X-ray amorphous; any identified crystalline phases are noted in Table 1 and Table 2. Thermal analysis has been performed only on those samples which have been confirmed to be XRD amorphous. DTA traces are shown in Figs. 2(a) and (b), with the extracted data of onset glass transition temperature (T_g), onset of first crystallization peak (T_r) and endotherm end-point liquidus temperature (T_{liq}) shown in Table 1 and Table 2. The value of ($T_r - T_g$), which is indicative of the thermal stability of glass, is illustrated in Fig. 3. Dilatometric measurements provide the coefficient of thermal expansion between 50 °C and 300 °C (α_{50-300}); the mid-point glass transition temperature (T_g); and the dilatometric softening point (T_d). Given that multiple crystalline phases occur in some glasses, T_{liq} corresponds to the highest-temperature endotherm, i.e. T_{liq} is the temperature above which no crystalline phases are present within the melt. Raman spectra are illustrated in Figs. 4(a,b); Fig. 5 shows selected fitted Mössbauer spectra and Fig. 6a and Fig. 6b illustrates the iron redox ratio measured by Mössbauer spectroscopy, as a function of (a) nominal modifier oxide content and (b) glass composition represented by the theoretical optical basicity calculated from analyzed compositions. Theoretical optical basicities have been calculated using published oxide basicity moderating parameters [39] and [40] and the analyzed composition of each glass. Estimated error bars shown in Fig. 6(b) include consideration of (i) errors associated with compositional analyzes and (ii) some Fe is present as FeO which has a different basicity moderating parameter to Fe_2O_3. Fig. 7 illustrates chemical durability as a function of nominal modifier oxide content.

Table 2. Nominal and analyzed composition and measured properties for $[(1 - x)\cdot(0.6P_2O_5–0.4Fe_2O_3)]\cdot xRO$ glasses.

Sample name	Mg10S	Mg20S	Ca10S	Ca20S	Ba10S	Ba20S	Ba30S	Ba40S	Ba50S	Pb10S	Pb20S	Pb30S	Pb40S
P_2O_5 mol% (analyzed)	49.08	40.00	49.08	40.00	49.08	40.00	32.30	25.71	20.00	49.08	40.00	32.30	25.71
	(53.2)	(47.6)	(53.9)	(48.0)	(56.1)	(49.3)	(42.5)	(36.3)	(29.2)	(51.9)	(44.8)	(38.0)	(31.3)
Fe_2O_3 mol% (analyzed)	32.72	26.66	32.72	26.66	32.72	26.66	21.54	17.14	13.33	32.72	26.66	21.54	17.14
	(35.1)	(28.8)	(34.7)	(30.0)	(33.5)	(29.8)	(26.3)	(22.0)	(17.0)	(33.6)	(29.3)	(25.3)	(21.6)
SiO_2 mol% (analyzed)	0 (0.2)	0 (0.2)	0 (0.2)	0 (0.2)	0 (0.3)	0 (1.5)	0 (1.5)	0 (2.7)	0 (4.7)	0 (0.9)	0 (0.2)	0 (0.7)	0 (1.1)
Al_2O_3 mol% (analyzed)	0 (0.1)	0 (0.1)	0 (0.1)	0 (0.1)	0 (0.4)	0 (1.1)	0 (1.5)	0 (2.3)	0 (2.8)	0 (1.1)	0 (0.9)	0 (1.4)	0 (1.7)
Na_2O mol% (analyzed)	0 (1.3)	0 (1.1)	0 (1.2)	0 (1.5)	0 (0)	0 (0)	0 (0)	0 (0)	0 (2.4)	0 (1.3)	0 (2.6)	0 (2.2)	0 (2.6)
K_2O mol% (analyzed)	0 (0.1)	0 (0.1)	0 (0.1)	0 (0.1)	0 (0.1)	0 (0)	0 (0.3)	0 (0.3)	0 (0.3)	0 (0.2)	0 (0.3)	0 (0.3)	0 (0.4)
MgO mol% (analyzed)	9.10 (10.0)	16.67 (22.0)	0 (0)	0 (0)	0 (0)	0 (0)	0 (0)	0 (0)	0 (0)	0 (0)	0 (0)	0 (0)	0 (0)
CaO mol% (analyzed)	0 (0)	0 (0)	9.10 (9.8)	16.67 (20.0)	0 (0)	0 (0)	0 (0)	0 (0)	0 (0)	0 (0)	0 (0)	0 (0)	0 (0)
BaO mol% (analyzed)	0 (0)	0 (0)	0 (0)	0 (0)	9.10 (9.6)	16.67 (18.4)	23.08 (27.8)	28.57 (36.2)	33.33 (42.3)	0 (0)	0 (0)	0 (0)	0 (0)
PbO mol% (analyzed)	0 (0)	0 (0)	0 (0)	0 (0)	0 (0)	0 (0)	0 (0)	0 (0)	0 (0)	9.10 (11.0)	16.67 (21.8)	23.08 (32.1)	28.57 (41.3)
SO_3 equivalent mol% (analyzed)	9.10 (0.042)	16.67 (0.058)	9.10 (0.030)	16.67 (0.072)	9.10 (0.023)	16.67 (0.023)	23.08 (0.115)	28.57 (0.219)	33.33 (1.355)	9.10 (<0.096)	16.67 (<0.101)	23.08 (<0.106)	28.57 (<0.109)
Phase/s identified	Am[b]	$Mg_2P_2O_7$ $Fe_3(PO_4)_2$ $FePO_4$	Am[b]	$FePO_4$	Am[b]	Am[b]	Am[b]	Am[b]	Unident. Phase/s	Am[b]	Am[b]	Unident. Phase/s	Unident. Phase/s
$\rho \pm 0.005$/g cm^{-3}	2.936	3.113	3.095	3.198	3.265	3.547	3.810	4.035	4.165	3.479	3.966	4.448	5.063
$V_m \pm$ 1/cm^3 mol^{-1}	46.58	39.66	44.75	40.20	45.50	41.68	38.78	36.33	34.09	44.42	40.86	38.10	34.66
($\alpha_{50–300} \times 10^{-7}$) ± 2/ ℃	73	n/m[a]	79	n/m[a]	73	87	97	104	n/m[a]	65	82	n/m[a]	n/m[a]
Dilatometric $T_g \pm 2$/ ℃	521	n/m[a]	524	n/m[a]	536	572	615	647	n/m[a]	506	508	n/m[a]	n/m[a]
Dilatometric $T_d \pm 2$/ ℃	548	n/m[a]	541	n/m[a]	567	595	637	693	n/m[a]	522	534	n/m[a]	n/m[a]
DTA mid-point $T_g \pm 2$/ ℃	526	n/m[a]	530	n/m[a]	547	582	616	n/m[a]	n/m[a]	518	525	n/m[a]	n/m[a]
DTA $T_r \pm 2$/ ℃	638	n/m[a]	658	n/m[a]	768	754	709	701	n/m[a]	630	625	n/m[a]	n/m[a]
DTA ($T_r - T_g$)/ ℃	123	n/m[a]	138	n/m[a]	230	178	102	43	n/m[a]	125	114	n/m[a]	n/m[a]
DTA $T_{liq} \pm 2$/ ℃	946	n/m[a]	988	n/m[a]	985	1019	1052	1051	n/m[a]	960	957	n/m[a]	n/m[a]
Mössbauer $Fe^{2+}/\Sigma Fe \pm 0.02$	0.211	n/m[a]	0.215	n/m[a]	0.185	0.266	0.258	0.254	0.214	0.211	0.255	0.258	n/m[a]
Mössbauer CS (Fe^{3+}) ± 0.02	0.39	n/m[a]	0.39	n/m[a]	0.38	0.39	0.40	0.37	0.43	0.39	0.39	0.40	n/m[a]
Mössbauer	0.91	n/m[a]	0.94	n/m[a]	0.92	0.94	0.91	0.88	0.81	0.91	0.90	0.88	n/m[a]

Sample name	Mg10S	Mg20S	Ca10S	Ca20S	Ba10S	Ba20S	Ba30S	Ba40S	Ba50S	Pb10S	Pb20S	Pb30S	Pb40S
QS (Fe^{3+}) ± 0.02													
Mössbauer CS (Fe^{2+}) ± 0.02	1.28	n/m[a]	1.26	n/m[a]	1.25	1.24	1.19	1.28	0.90	1.28	1.25	1.24	n/m[a]
Mössbauer QS (Fe^{2+}) ± 0.02	2.07	n/m[a]	2.10	n/m[a]	2.09	2.02	2.13	1.85	2.64	2.14	2.13	2.13	n/m[a]

[a] n/m, Not measured.

[b] Am, amorphous.

4. Discussion

4.1. Composition, density, molar volume and crystallinity

It is often useful to numerically represent glass composition and structure in some meaningful way when considering the effects of methodical changes in composition, as we have studied here. Several such scales exist, although all have their limitations. Previously when studying the sulfur capacity of these and other glasses [34] we have considered simple scales such as P_2O_5content or [O]/[P] ratio in addition to more complex, and arguably more meaningful, scales such as theoretical optical basicity [39]and [40] or cation field strength index [41]. In this paper with one exception we have presented the majority of our results in terms of nominal modifier content as the clearest means to illustrate the effects of different modifiers upon the properties of interest.

Increasing modifier oxide contents lead to higher levels of contamination of the final glass by SiO_2 and Al_2O_3 arising from increased dissolution of the mullite crucibles in which they have been prepared. This is consistent with the behavior of high-flux glass melts, i.e. those rich in alkali and alkaline earth oxides. As we have noted previously, the corrosivity of $60P_2O_5$–$40Fe_2O_3$melts towards alumina and aluminosilicate refractories are remarkably low by comparison with the effects of other phosphate glass melts [35].

Densities and molar volumes are shown in Table 1 and Table 2 and as a function of nominal modifier oxide content in Fig. 1(a). Only additions of BaO and PbO act to strongly increase density, reflecting the high mass of their constituent cations. In particular it may be noted that the alkali additions studied here have little effect on final glass density. In general the molar volumes, V_m, of the different samples gradually decrease with increasing modifier oxide addition, as illustrated in Fig. 1(b). The addition of K_2O appears to result in a more voluminous glass structure than occur for glasses containing other additions. Our results for the effects of Na_2O and K_2O additions on density and molar volume are consistent with those obtained by Fang et al. [19] for similar glasses.

X-ray diffraction (XRD) measurements reveal the limits of glass formation, which have been discussed and illustrated previously [34]. The identified crystalline phases which occur when the glass formation region has been exceeded are noted in Table 1 andTable 2. Phases arising in materials containing heavier oxides (K_2O, BaO, and PbO) have not been positively identified using standard powder diffraction files. Heavier modifier cations substantially extend the glass formation region [34], therefore it is likely that the primary phase/s for samples in which crystallization occurs during cooling are rich in modifier cations.

4.2. Thermal properties

The addition of increasing levels of modifier cations, both monovalent and divalent, generally has the effects of (a) increasing $T_g$and (b) increasing T_{liq}. The effects upon the other measured parameters are varied. These comprise coefficient of thermal expansion, $\alpha_{50–300}$, dilatometric softening point, T_d, and the onset temperature of bulk crystallization, T_r, and therefore thermal stability, which can be illustrated by the magnitude of (T_r–T_g).

The addition of alkali oxides to the base formulation, PFe1 M, produces only small increases in T_g, even at 30 mol% alkali oxide (see Table 1 and Fig. 2). This is consistent with the results of Marasinghe et al. [17], who studied *pro rata* additions of up to 20 mol% Na_2O and up to 30 mol% Cs_2O to the same base glass that we have studied here. Alkali additions strongly increase α_{50-300}, the coefficient of thermal expansion between 50 °C and 300 °C. This has the effect of making the glass less resistant to thermal shock. The value of $(T_r - T_g)$, which can be used as a measure of the thermal stability of a glass, is consistent with the glass formation boundaries within the respective systems. For example, as shown in Fig. 3, sample Li10S exhibits a lower $(T_r - T_g)$ than the base glass PFe1 M since it is close to its glass formation boundary which occurs between 10 and 20 mol% Li_2O [34]. However, the addition of Na_2O and K_2O results in substantially greater glass forming capabilities. This is reflected in the fact that $(T_r - T_g)$ remains largely unchanged up to 20 mol% Na_2O and K_2O, then decreases at 30 mol% (see Fig. 3). This is again consistent with our earlier results [34] which suggest that the glass formation limit, i.e. when a sample is cooled in air and the formation of crystallinity can be detected by XRD analysis, can be described by a broadly linear relation between the modifier cation field strength, $\sum z/a^2$, and the atomic percentage of modifier cation. The effects of alkali additions upon T_d, which corresponds to viscosities of 10^9–10^{10} dPa s [42], are consistent with their known effectiveness in decreasing high temperature viscosity in the order Li < Na < K [43].

As we have discussed in a previous publication [10], the main exotherms in the DTA trace for the base glass, PFe1 M, which are centered at approximately 650 °C and 850 °C, have been attributed by Day and co-workers to the crystallization of $Fe^{2+}Fe_2^{3+}(P_2O_7)_2$ and $Fe_4(P_2O_7)_3$, or ferrous-ferric pyrophosphate and ferric pyrophosphate, respectively. DTA traces for samples doped with alkalis all suggest that the former, lower-temperature phase $Fe^{2+}Fe_2^{3+}(P_2O_7)_2$ is the primary phase for these materials. Similar thermal characteristics are exhibited by Li_2O, Na_2O, and K_2O, albeit depending upon (a) the amount of modifier added and (b) the proximity of that composition to its respective glass formation boundary. Therefore the traces for (i) Li10S, Na30S and K30S; (ii) Na10S and K10S; (iii) Na20S and K20S bear similarities due to the parameters (a) and (b) described above. These similarities are also reflected in the value of $(T_r - T_g)$ as shown in Table 1. Hence we may conclude that the thermal stabilities of the alkali-doped glasses are proportional to a combination of the two factors, (a) and (b). Glasses are more stable, for a given molar addition of alkali, with increasing alkali cation size in the series Li < Na < K. One may speculate that this series can be extended to include Rb and Cs. Marasinghe et al. [17] observed that the addition of Cs_2O to a $60P_2O_5$–$40Fe_2O_3$ (mol%) base glass suppresses crystallization at low Cs_2O additions but enhances it at high concentrations, whereas Na_2O promotes crystallization and sharpens crystallization peaks. This behavior is also consistent with the effects of each different alkali addition upon the glass formation boundary.

Thermal analysis data for glasses doped with divalent cations display behavior that is somewhat more mixed than for samples containing alkali additions. At one end of the scale lie samples doped with Mg or Pb, which broadly exhibit behavior similar to that caused by the addition of comparable molar quantities of monovalent oxides. Glasses doped with Ca and Ba, respectively display moderately and markedly different behavior to alkali-doped glasses. Their additions to the base glass cause partial (Ca) and full (Ba) suppression of the crystallization peak at 600–700 °C in favor of the higher-temperature crystallization peak in the range 700–800 °C. These effects are accompanied by comparative increases in T_g, T_d and T_{liq}. With the addition of BaO, T_g increases substantially whilst the low-temperature exotherm found at ~655 °C in the base glass PFe1 M, is suppressed and the high temperature exotherm at 700–800 °C decreases in temperature. The overall effect of this is to initially increase $(T_r - T_g)$ by 100 °C whilst only increasing T_{liq} by 35 °C, resulting in substantially greater thermal stability of sample Ba10S than the base glass (sample PFe1 M). Further BaO additions continue to increase T_g, decrease T_r and increase T_{liq}, however, glass stability remains better than or comparable to that of the base glass at levels of up to 30 mol% BaO. Only at 40 mol% BaO does the thermal stability decrease sharply as a result of $(T_r - T_g)$ approaching zero, which is indicative of proximity to the glass formation boundary. We therefore conclude that our P_2O_5–Fe_2O_3–BaO glasses display good thermal stability at all but the highest BaO additions and this stability, coupled with other beneficial effects of adding BaO, recommend these glasses for a number of potential applications. In addition to imparting high thermal stability, the addition of divalent cations such as Ba^{2+} imparts a moderate increase in thermal expansion which is in line with expectations [43], but which is less marked than the increases associated with alkali additions, as shown in Table 1 and Table 2. This is consistent with divalent cations being more tightly bound within the matrix owing to their greater field strength.

The substantial differences in the value of (T_r-T_g) which occur upon addition of the various modifiers studied here imply that large shifts in the main crystallization peak result from the formation of different crystalline phases, i.e. shifts in the primary phase field. This would be expected on the basis of the substantial compositional changes with which they are associated. Our summation is corroborated by the differences in stoichiometry of those phases which form outside the glass formation region, as identified inTable 1 and Table 2.

In general, increasing additions of modifiers to the base glass increases α_{50-300}, T_g, T_d and T_{liq}. This behavior is broadly consistent with that observed by other researchers for similar phosphate glasses [29], [30] and [33]. The increase in T_g is probably due to the decrease in average value of Q with increasing modifier oxide content, discussed in Section 4.3.1. Although the base glass is strongly depolymerized, further depolymerization clearly takes place upon addition of modifiers and this replacement of P–O–P bonds by P–O–M bonds contributes to the increases in T_g and T_d. An increasing modifier content results in an increase in cross-linking density between phosphate units (although this effect is limited by the short average length of phosphate units as discussed in Section 4.3.1). The increase in α_{50-300} with increasing modifier content would appear to dispute this structural assertion, as thermal expansion is also strongly influenced by the strength of network bonding, its connectivity and the interactions between cations and non-bridging oxygens. However, others [33] have also observed similar trends in modified iron phosphate glasses. It is noted that, for our glasses, distinct differences occur between the effects of monovalent and divalent modifiers. Monovalent modifiers generally have only a small effect on T_g but strongly increase α_{50-300}, whereas divalent modifiers, in general, strongly increase T_g but have a more moderate effect on α_{50-300}. As expected, this is indicative of network bonding and connectivity being more strongly increased by divalent modifiers than monovalent modifiers, and is consistent with the greater field strength and M–O bond strength of divalent modifiers. An additional factor to consider is that iron redox does not change linearly with modifier content. In addition the Fe–O bond strengths and local structural environments of Fe^{2+} and Fe^{3+} cations in the phosphate network are not identical owing to differences in ionic radius and ionic charge, notwithstanding any small differences in coordination which may occur. As discussed in Section 4.3.2, Mössbauer analyzes reveal substantial changes in the $Fe^{2+}/\Sigma Fe$ redox ratio with changing modifier content but do not indicate large differences in coordination of Fe^{2+} and Fe^{3+} ions. Changing redox ratio may therefore be involved in the observed trends in α_{50-300}, T_g, T_d and T_{liq}. We must also consider the fact that as modifiers are added to our base glass, the content of P_2O_5 and Fe_2O_3 are decreased. This is reflected in the fact that, for a given modifier type, T_g increases to a maximum value but further modifier additions result in a decrease in T_g. It therefore seems likely that the competing factors of reduced P_2O_5 content (which will act to reduce the average Q), reduced Fe_2O_3 content (which will act to increase the average Q), increased modifier content (which will act to reduce the average Q and change the M–O bond strength depending upon amount and type of modifier) and changes in the iron redox ratio, are responsible for the trends shown in T_g and any apparent discrepancies between the effects of a strengthened network and the increases in both T_g and α_{50-300}. Clearly these relationships are not yet fully understood for phosphate glasses and further research is required in this area.

4.3. Structural analysis

4.3.1. Raman spectroscopy

As shown in Fig. 4(a,b), Raman peaks occur at ~340 cm^{-1}, ~630 cm^{-1}, ~750 cm^{-1}, ~950 cm^{-1}, ~1080 cm^{-1} and ~1250 cm^{-1}in the base glass, PFe1 M. This spectrum is consistent with published spectra for similar glasses [17] and [44]. There is some (although not comprehensive) agreement in the literature that iron phosphate glasses similar in composition to ours consist of a highly depolymerized phosphate network. On the basis of the literature consensus, where it exists, we have made the following band assignments for our spectra:

- ~350 cm^{-1} bending of (PO_4) units with Fe as modifier
- ~760 cm^{-1} symmetric stretching of (P–O–P) bonds in Q^1 $(P_2O_7)^{4-}$ units
- ~950 cm^{-1} asymmetric stretching of Q^0 $(PO_4)^{3-}$ monomer units
-

~1080 cm^{-1} asymmetric stretching of Q^1 $(P_2O_7)^{4-}$ dimer units

- ~1250 cm^{-1} asymmetric stretching of Q^2 $(PO_3)^-$ metaphosphate units

Additions of modifier cations to the base glass, PFe1 M, result in a number of spectral changes which become more pronounced as the modifier content increases, as illustrated in Fig. 4(a,b). These changes are summarized below.

- ~350 cm^{-1} shifts to lower energies
- ~470 cm^{-1} new band emerges; increases in intensity
- ~630 cm^{-1} increases in intensity
- ~760 cm^{-1} decreases in intensity
- ~950 cm^{-1} becomes consumed by the broad ~1080 cm^{-1} band as it shifts to lower energies
- ~1080 cm^{-1} shifts to lower energies; broadens; splits into 2 distinct bands at ~1000 cm^{-1} and ~1100 cm^{-1}
- ~1250 cm^{-1} shifts to lower energies/disappears

Some of the effects of modifier content on Q-species of phosphate glasses have been discussed elsewhere [45], [46], [47], [48],[49] and [50], following pioneering work by Van Wazer [51]. The new band at ~470 cm^{-1} may arise from Q^0 $(PO_4)^{3-}$ units [52]. This suggestion is supported by interpretation of spectra for P_2O_5–Fe_2O_3–PbO–Na_2O glasses by Moguš-Milanković et al. [53] who claim that their band at ~470 cm^{-1} arises from O–P–O bending modes of Q^0 units. It might be suggested that the 'disappearance' of the peak at ~925 cm^{-1} is related to the conversion of $Q^0(PO_4)^{3-}$ monomer units into more polymerized phosphate units. However, close examination of this peak indicates that rather than disappearing, the peak becomes consumed by the broad band at higher energies as that band shifts to lower energies. Furthermore, as the band at ~470 cm^{-1}, which grows in intensity with modifier addition, is also attributed to $Q^0(PO_4)^{3-}$ monomer units it seems more likely that the number of $Q^0(PO_4)^{3-}$ monomer units increases with modifier addition. The gradual decrease in intensity of the (relatively weak) band at ~760 cm^{-1} with increasing levels of modifier addition also indicates the partial conversion of $Q^1(P_2O_7)^{4-}$ dimer units into other phosphate units. It seems clear that the main peak centered at ~1080 cm^{-1} comprises a number of overlapping components which cause the overall band position and profile to shift as a function of modifier addition. We view the origin of this broad peak as a distribution of Q^0, Q^1 and Q^2 phosphate groups. Shifts in the overall band position and shape are therefore indicative of changes in the distribution of Q-species. A shift towards lower energies represents a more depolymerized network, i.e. a lower average value of Q. Therefore the addition of modifiers to the base glass results in a decrease in average Q.

A Raman band at ~630 cm^{-1} observed in spectra for P_2O_5–Fe_2O_3–FeO–Cs_2O glasses [23] and for other iron phosphate glasses[28], [52] and [53], has previously been attributed to symmetric stretching of bridging oxygens $(P–O–P)_{sym}$ in Q^2 species. Those authors state that the band is indicative of Q^2 species arising from disproportionation of Q^1 species to Q^0 and Q^2 species. Literature for a range of modifier-containing phosphate glasses shows a commonly-occurring band centered at ~690 cm^{-1} with a broad tail stretching towards higher Raman Shifts [21], [47], [54] and [55]. This band has also been attributed to symmetric stretching of bridging oxygens $(P–O–P)_{sym}$ in Q^2 species. The Raman Shifts and band shapes for the band at ~630 cm^{-1} in our spectra are substantially different from the ~690 cm^{-1} bands, and these differences are, in our opinion, too great for the two bands to have the same structural origin. One publication discussing modified iron phosphate glasses notes the presence of a Raman band at ~650 cm^{-1} and attributes it to dimer units, i.e. $Q^1(P_2O_7)^{4-}$ units [17]. We suggest that this is also unlikely for our glasses, given the partial conversion of $Q^1(P_2O_7)^{4-}$ dimer units into other phosphate units discussed in the previous paragraph. We do note, however, that the Raman band at ~630 cm^{-1} increases in intensity proportionately with the band at ~470 cm^{-1} with increasing modifier oxide content (see Fig. 4(a,b)). The facts that this behavior occurs with all of the different modifiers that we have studied, and others [23], and that both bands behave proportionately, suggests that they have similar structural origins.

The spectral changes that take place as a function of modifier content are primarily governed by the level of addition and, as described above, the glass structure shifts towards a more depolymerized matrix with a lower average value of Q^i upon modifier addition. However, structural differences also occur, albeit to a less pronounced degree, when comparing the effects of different modifiers at a given molar percentage. For example, Raman spectra for K_2O- and BaO-doped glasses, which are shown in Fig. 4(a,b), respectively, clearly exhibit structural differences at the same nominal molar oxide addition. Differences are most noticeable when comparing the effects of monovalent and divalent cations and any differences between, for example, Na_2O and K_2O or CaO and BaO, are consistently small. This behavior is consistent with the differing effects of alkalis and divalent cations on the structure of phosphate glasses.

4.3.2. ^{57}Fe Mössbauer spectroscopy

Fitted values of Center Shift (CS) and Quadrupole Splitting (QS), shown in Table 1 and Table 2, are similar to published values for other iron phosphate glasses [6], [7], [9], [10], [12], [13], [15], [17], [18], [20], [31] and [32] and are consistent with the conclusion that both Fe^{2+} and Fe^{3+} predominantly occupy a range of distorted octahedral sites in all of the modified iron phosphate glasses studied here. Sites with lower coordination numbers may also be present; however, the Mössbauer results indicate that their abundance is relatively low. X-ray absorption spectroscopy, neutron diffraction and X-ray diffraction studies of a range of binary, ternary and modified iron phosphate glasses have provided average Fe–O coordination numbers from 4.8 to 5.5 [15], [16], [17],[18], [56], [57], [58], [59], [60] and [61] indicating the presence of some 4-coordinated and/or 5-coordinated iron. It should be noted that it is very difficult to separate the contributions from Fe^{2+} and Fe^{3+} using these spectroscopies and instead an 'average' is generally obtained. Debate still exists as to the detailed environments of Fe^{2+} and Fe^{3+} in iron phosphate glasses. For example, Wright et al. [61] recently noted that their neutron diffraction results mitigate against the presence of large numbers of the $(Fe_3O_{12})^{16-}$ clusters that are postulated by the structural model of Marasinghe et al. [56].

Hyperfine parameters obtained from fitting of our Mössbauer spectra indicate that, within the range of glasses surveyed, glass composition does not have a large effect on the local environment of the Fe^{2+} and Fe^{3+} cations. Again, our results are consistent with those from other studies of iron phosphate glasses which have concluded that the near-neighbor local environment of iron is not greatly affected by the addition of modifier cations [16], [17], [18], [56], [57], [58], [59] and [60].

The redox ratio, $Fe^{2+}/\Sigma Fe$, is substantially affected by the abundance and type of modifier addition as illustrated by the variation in fitted spectra shown in Fig. 5. As also shown in Fig. 6(a), $Fe^{2+}/\Sigma Fe$ increases upon initial addition of all modifiers, reaching a maximum value at roughly 20 mol% R_2O or 30 mol% RO addition, and above these levels $Fe^{2+}/\Sigma Fe$ decreases with further modifier additions. This behavior is illustrated more clearly by Fig. 6(b), in which theoretical optical basicity, Λ_{th}, is plotted as an indicator of composition/structure. In addition to our own data we have also calculated the redox behavior of the glasses investigated by Marasinghe et al. [16] and [17], which came from ostensibly the same family of glasses as ours, i.e. $[(1-x)\cdot(0.6P_2O_5–0.4Fe_2O_3)]\cdot xR_xO_y$, where their R = Na, Bi, Ca, and Cs. We note that Marasinghe et al. neglected to consider differences in Fe^{2+} and Fe^{3+} recoil-free fraction ratios in their Mössbauer fitting, which affects the redox ratio measurement. We have converted their data for the purposes of this examination using the same method that we have applied to our own data (see Experimental). Marasinghe et al. also used different melting programmes to ours: in [16] their glasses were melted at approximately 1150 °C for 1–2 h and were apparently unstirred. In [17], their glasses were melted at approximately 1200 °C for 1–2 h and again the melts were apparently unstirred. Our glasses were melted at exactly 1150 °C for 3 h, and were stirred during melting to improve homogeneity. Differences in iron redox ratios between our glasses and comparable glasses of Marasinghe et al. (e.g. the base glass and the Na_2O-doped series) can be attributed to differences in preparation and particularly to the effects of different melting temperatures, which have been assessed in another publication [44]. Despite these differences, the data of Marasinghe et al. [16] and [17] exhibits the same trend in redox as a function of composition as our data (see embedded graph inFig. 6(b)), adding further support that the trends shown by our data are reproducible.

To explain the redox behavior of $[(1-x)\cdot(0.6P_2O_5–0.4Fe_2O_3)]\cdot xR_xO_y$ glasses with increasing x we must first consider any potential involvement of the sulfate that was present in our batches and which predominantly or completely volatilized during melting, presumably as SO_2 and $½O_2$[62]. The measured redox ratio, $Fe^{2+}/\Sigma Fe$, for samples Na20 (prepared using batch Na_2CO_3) and Na20S (prepared using batch Na_2SO_4) are equal within errors of measurement and fitting (see Table 1). This strongly supports the argument that the carbonate and sulfate batch materials that we used have the same effect

on final glass redox, within experimental parameters. Therefore we can discount significant involvement of batch sulfate in the redox processes observed. This conclusion is also supported by the results of Marasinghe et al. [16] and [17], illustrated as the embedded graph in Fig. 6(b), since those authors did not use batch sulfates but presumably used carbonates or oxides to supply their modifiers, and yet their data exhibits the same behavior.

It is known that in simple oxide melts the $M^{m+}/M^{(m+n)+}$ ratio, where M is a multivalent ion present in dilute quantities, generally decreases as the melt composition becomes more basic [63], [64] and [65], i.e. as the ability of constituent O^{2-} to donate negative charge becomes greater. This behavior can be described by the optical basicity concept developed by Duffy and Ingram [39], [40]and [63], and which we have used here to illustrate our glass compositions across a range of modifier types and additions (Fig. 6(b)). In some cases, changing glass basicity does not adequately explain the redox behavior in glasses of iron [66] and [67] and certain other multivalent species [68], [69], [70], [71] and [72]. Others have also noted that redox behavior may involve other factors than glass basicity [63] and [65]. A similar trend to that which we have noted, i.e. a maximum value of $M^{m+}/M^{(m+n)+}$ occurring at intermediate modifier contents and hence intermediate glass basicities, has also been observed for dilute (1 wt%) quantities of iron in sodium silicate and alkali borosilicate glasses by Schreiber et al.[67]. Their explanation for this deviation from the trend predicted by glass basicity (i.e. $M^{m+}/M^{(m+n)+}$ decreases with increasing basicity) is that a change in coordination of Fe^{3+} takes place. They state that Fe^{3+} occupies octahedral sites in acidic glasses, whereas in basic melts it converts to FeO_2^- occupying tetrahedral sites. However, they present no measurements of the structural role of iron in their own glasses to support their assertion. Similar redox behavior has again been observed in the $Cu^{2+}/\Sigma Cu$ ratio of P_2O_5–CuO–(Cu_2O) glasses as a function of CuO content by a number of independent research groups [66], [67], [68] and [69]. Some authors have, like Schreiber et al.[67], attempted to explain this behavior by a change in transition metal ion coordination as a function of glass composition [70] and [71]. Bih et al. [72] studied the effects of Li_2O/P_2O_5 ratio and MoO_3 content on the $Mo^{5+}/\Sigma Mo$ redox ratio in Li_2O–MoO_3–P_2O_5 glasses. They observed that, when $(MoO_3)_2$ content was constant at 5 mol%, the ratio $Mo^{5+}/\Sigma Mo$ decreased with increasing Li_2O content. This is consistent with the accepted view of redox behavior as per the basicity model [39] and [40]. However, for their second series of glasses, when the Li_2O content was constant and the MoO_3/P_2O_5 ratio varied, a trend in $Mo^{5+}/\Sigma Mo$ occurred similar to that which we (and others [67]) have observed for $Fe^{2+}/\Sigma Fe$. Paul and Douglas' early publication on the Fe^{2+}/Fe^{3+} equilibrium in binary alkali silicate glasses [73] again describes a similar trend to ours. However, this trend only occurred for those glasses which they melted in Pt crucibles and Pt was believed to have an oxidizing effect on the Fe redox equilibrium in glasses containing less than ~30 mol% R_2O (R = Li, Na, and K). In glasses melted in ceramic crucibles the Fe redox behavior followed a pattern consistent with that predicted by glass basicity.

In addition to its usefulness in determining the oxidation state, Mössbauer spectroscopy is a powerful tool for studying changes in the local structural environment of Fe in glasses [74], [75] and [76]. Our fitted center shift (CS) and quadrupole splitting (QS) values do not support a substantial change in Fe^{3+} coordination as a function of increasing modifier content or increasing glass basicity. Instead, CS (Fe^{3+}) and QS (Fe^{3+}) remain remarkably consistent for all types and levels of modifier addition. Small, subtle deviations are observed for some samples but these are insufficient to explain the observed redox trend shown in Fig. 6a and Fig. 6b and described in Table 1 and Table 2. The evidence from Mössbauer spectroscopy therefore casts doubt on the suggestion made by several other authors that the observed redox behavior is attributable to changes in Fe^{3+} coordination, and as a result we must consider alternative explanations. One is that the observed redox phenomenon has a structural origin and is related to the polymerization and speciation of the network and the thermodynamic stability of different structural units as a function of composition, rather than being solely governed by classical redox reactions. There is support for such a hypothesis, given the high iron content of the glasses in which iron is a major constituent rather than a solute. As shown by thermal analysis (see Section 4.2) the glass stability defined as ($T_r - T_g$) varies greatly. Some of the crystalline species associated with exothermic DTA peaks have previously been identified by Day and co-workers as containing all Fe^{3+} or a mixture of Fe^{2+} and Fe^{3+}, as we have discussed previously [10]. Therefore it is possible that the iron redox ratio is inextricably linked to glass stability in these systems. This hypothesis would therefore suggest that the redox ratio in iron phosphate glasses can vary to an extent in order to fulfil the requirements of glass stability, and vice versa. Further investigation of this behavior is suggested.

4.4. Chemical durability

Leach test results arising from 7-day Product Consistency Test B (PCT-B) testing at 90 °C [37], and illustrated in Fig. 7, reveal a number of important trends.

- (i) For a given molar alkali content, durability decreases in the order Na < K.
- (ii) Addition of K_2O has no effect on durability at levels up to 20 mol%. Durability then decreases with further increases in K_2O content.
- (iii) Durability decreases with increasing Na_2O content.
- (iv) Divalent oxide additions improve durability. Addition of BaO produces the greatest improvement.
- (v) All glasses exhibit good to excellent aqueous durability. Even high-alkali (40 mol% R_2O) samples exhibit leach rates that are still comparable to those exhibited by the surrogate waste-loaded borosilicate glasses.

Chemical durabilities, measured by PCT-B, are plotted in Fig. 7 as functions of the nominal modifier oxide content of each sample. In addition to results for the modified iron phosphate glasses, PCT-B results for the commercial SLS container glass and for the surrogate waste-loaded borosilicate glass MW, used to immobilize the UK's high-level nuclear waste (HLW) [36], have been included. The base glass, PFe1 M, has a low optical basicity and each incremental increase in modifier addition has the effect of increasing optical basicity.

As shown in Fig. 7, glasses containing additions of divalent cations, and particularly BaO and PbO, exhibit aqueous leach rates of ~0.0001 g m^{-2} d^{-1} at 90 °C. Such leach rates are exceptionally low, and are comparable with those obtained from testing of the best ceramic waste immobilization host materials that are presently available [77]. However, further research must be conducted under a range of test conditions including long-term leaching behavior and the effects of pH before one can definitively state that these glasses out-perform alkali borosilicate glasses under likely repository conditions.

The addition of modifier ions to phosphate glasses is known to strongly affect their chemical durability. For example, Bunker et al.[78] demonstrated that the durability of P_2O_5–R_2O–RO glasses is considerably improved, over a range of pH values, following replacement of alkali oxides by alkaline earth oxides and following replacement of Na_2O by Li_2O. Peng and Day [79] studied the effects of Na_2O and K_2O in R_2O–R_2O_3–P_2O_5 glasses, noting that ionic cross-linking between non-bridging oxygens (NBO's) is provided by alkali and alkaline earth cations, and increasing the bond strength of this ionic crosslink is expected to improve chemical durability. They stated that since ionic radius increases in the order Li^+ < Na^+ < K^+ the crosslink strength decreases in the same order, so that chemical durability of their glasses decreased in the order Li > Na > K. Minami and Mackenzie [80] and Metwalli and Brow [81] have observed similar effects in R_2O–Al_2O_3–P_2O_5 glasses, which are broadly appropriate as structural comparators for our alkali-modified iron phosphate glasses.

Other studies by Shih and Shiu [82], Shyu and Yeh [83] and Jung et al. [84] document the effects upon chemical durability of phosphate glasses containing no alkalis by replacing high field strength modifiers by low field strength modifiers. In these works the trend exhibited by replacing alkalis discussed above is different. For example, Shih and Shiu [82] replaced ZnO by SrO in P_2O_5–SrO–ZnO glasses and observed a substantial increase in durability as SrO replaced ZnO. Similarly, Jung et al.[84] observed the same trend for as BaO replaced ZnO in P_2O_5–BaO–ZnO glasses. Metwalli and Brow [81] observed a similar increase in durability upon replacing MgO by BaO in P_2O_5–Al_2O_3–RO glasses.

The behavior of our glasses upon addition of the alkalis Li_2O, Na_2O and K_2O is not consistent with the evidence described above which indicates that durability should increase with increasing field strength (i.e. decreasing size) of the alkali cation. As a result the fact that durability of our modified iron phosphate glasses increases in the order Li < Na < K for a given molar content of R_2O is unexpected, based on the known effects of alkali ionic radius on the durability of other phosphate glasses. The effects of divalent additions upon durability are more consistent with the literature evidence discussed above. However, existing structural and mechanistic models do not fully explain this behavior. As noted by an anonymous reviewer in a comment with which we fully concur, the relationships between modifier ion properties and

phosphate glass durability are not well understood, but it seems clear that the simple field strength arguments are quite inadequate.

The behavior of K_2O in iron phosphate glasses is interesting because durability only begins to decrease >20 mol% K_2O. Assessment of the Raman spectra for this series of glasses indicates that any structural differences (in terms of the degree of depolymerization) between glasses containing equimolar amounts of Li_2O, Na_2O and K_2O are not large. However, molar volumes shown in Fig. 1(b) indicate that K_2O glasses maintain a voluminous structure by comparison with the other glasses, even those containing other alkalis such as Na_2O. Further work, possibly using X-ray or neutron techniques, would be useful to obtain more information on any structural differences which may explain these apparently unusual trends in chemical durability.

Lead–iron phosphate glasses were investigated in the 1980s by Sales and Boatner [3], who observed their high aqueous durabilities accompanied by melting and processing temperatures as low as 800 °C. However, as outlined by Jantzen [1], a number of problems beset the lead–iron phosphate glass formulations that had been developed (typically 35–55 mol% P_2O_5, 30–55 mol% PbO and 10 mol% Fe_2O_3). These problems included low waste loading capacities, high melt corrosivity, incompatibility with certain canister materials and poor thermal stability. Furthermore, chemical durability when tested under extreme conditions at 200 °C in 7 M NaCl solution, was found to be very inferior to the durability of borosilicate waste glasses [85]. Our P_2O_5–Fe_2O_3–PbO glasses differ substantially from those developed by Sales and Boatner [3]. We regard their glasses as lead phosphate glasses doped with iron since the Fe_2O_3 contents are relatively low. Our glasses, on the other hand, may be regarded as iron phosphate glasses doped with lead: a minor-sounding difference but a compositionally significant one. According to Jantzen [1], the lead–iron phosphate glasses of Sales and Boatner suffer from rapid thermal devitrification at temperatures above 550 °C. By comparison, our DTA traces illustrated in Fig. 2(b) for glasses Pb10S and Pb20S (10 and 20 mol% PbO, respectively) indicate that at 550 °C there is no crystallization tendency, indeed the crystallization exotherms do not even begin until 675 °C and 630 °C respectively. It seems clear that the addition of PbO, whilst it substantially decreases viscosity and melting temperature, also decreases glass stability in iron phosphate glass systems. Combined with the fact that samples Pb30S and Pb40S exhibited some crystallization upon cooling, it might be prudent to limit the addition of PbO to the $60P_2O_5$–$40Fe_2O_3$ base glass to 20 mol%.

Barium doped iron phosphate glasses have received limited attention as potential host materials for the immobilization of surplus PuO_2[86]. The authors provided little detail but it seems likely that the addition of BaO to their base glass provided some benefits when immobilizing PuO_2, otherwise there would be no reason to do so. More widely, barium-rich phosphate glasses generally exhibit high chemical durabilities [80] and [84] which lends further support to their investigation as a potential host material for waste immobilization. Our results for barium-doped iron phosphate glasses substantially support the use of barium. Not only is the capacity of the base glass to incorporate BaO the highest of all the additions studied (40 mol% BaO produces a fully amorphous glass when cast in air), but its effect is to increase aqueous durability to the point at which leach rates for the PCT-B test are at or below the limits of detection for the ICP-OES technique that we have used. The absence, to our knowledge, of any prior determination of the behavior of P_2O_5–Fe_2O_3–BaO glasses with these compositions mark our discovery and development of these new, ultra-durable, thermally stable, low-melting glasses as a significant step forward. Clearly more development and testing remains to be carried out, but this important discovery could prove to be useful for a range of glass applications including, but not restricted to, waste immobilization.

5. Conclusions

Molar additions of monovalent (Li, Na or K) or divalent (Mg, Ca, Ba, and Pb) oxides to a 60 mol% P_2O_5–40 mol% Fe_2O_3 (nominal) glass result in substantially different effects on thermal properties and chemical durability. The addition of up to 40 mol% R_2O has relatively little effect on density, T_g and T_d; however, addition of RO increases these parameters proportionately to the level of addition. Both monovalent and divalent additions result in increases in α_{50-300} and T_{liq}.

The iron redox ratio, $Fe^{2+}/\Sigma Fe$, exhibits a complex relationship with glass composition, with a maximum value occurring at intermediate levels of modifier addition (corresponding to ~20 mol% R_yO). This behavior has, to our knowledge, been rarely observed in oxide glasses and does not conform to conventional linear relationships established for relatively simple glasses doped with dilute quantities of iron. Previous explanations for similar behavior were given on the basis of changes in iron coordination. However, fitted Mössbauer parameters show that iron coordination does not change across the range of compositions studied here, therefore changes in iron coordination are not responsible for the redox behavior. An alternative hypothesis based on structural requirements is suggested.

The effects of R^+ and R^{2+} cations upon chemical durability, measured by Product Consistency Test B (PCT-B), are markedly different. Alkali additions decrease chemical durability, although durability for a given molar addition increases through the series Li < Na < K. Even high (30–40 mol%) R_2O additions result in glasses with durabilities no worse than those of commercial SLS glass and a surrogate nuclear waste-loaded borosilicate glass. On the other hand, addition of divalent cations consistently increases durability to a level even greater than the high durability displayed by the base glass. Log (dissolution rate/g m^{-2} d^{-1}) having values of –3 to –4 have been recorded for all divalent additions (Mg, Ca, Ba, and Pb), even 40–50 mol% in the cases of Pb and Ba. Taking all the results together the P_2O_5–Fe_2O_3–BaO glasses reported here show particular promise as they are ultra-durable, thermally stable, low-melting glasses with a wide glass formation region.

The capacity of the base glass to incorporate R^+ and R^{2+} cations, and particularly large cations with low field strengths, is substantial. Highly-modified glasses containing R^{2+} cations generally exhibit high aqueous durabilities which are greater than the durability of the base glass, which is itself very high. As a result, some of the modified iron phosphate glasses studied here might find applications as hosts for nuclear or toxic wastes rich in R^+ or R^{2+} cations and in particular, large cations with low field strengths, particularly Ba^{2+} and Pb^{2+}.

Acknowledgements

The authors acknowledge with thanks EPSRC, the UK's Engineering and Physical Sciences Research Council, for funding this research. The authors also wish to acknowledge two anonymous reviewers for their suggestions and constructive comments.

Figures

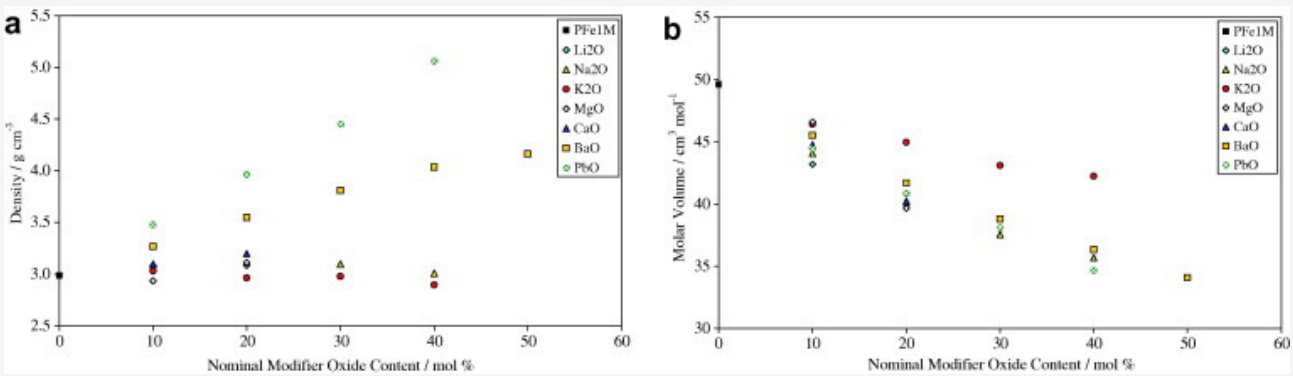

Fig. 1. (a) Density and (b) molar volume as a function of nominal modifier oxide content for $[(1-x)\cdot(0.6P_2O_5–0.4Fe_2O_3)]\cdot xR_yO$ glasses.

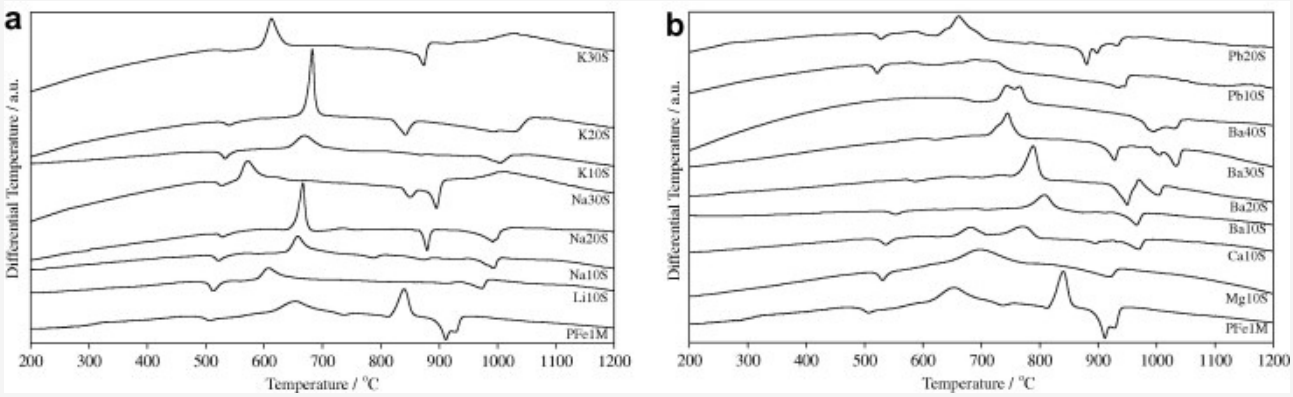

Fig. 2. DTA curves of (a) $[(1-x)\cdot(0.6P_2O_5–0.4Fe_2O_3)]\cdot xR_2O$ and (b) $[(1-x)\cdot(0.6P_2O_5–0.4Fe_2O_3)]\cdot xRO$ glasses.

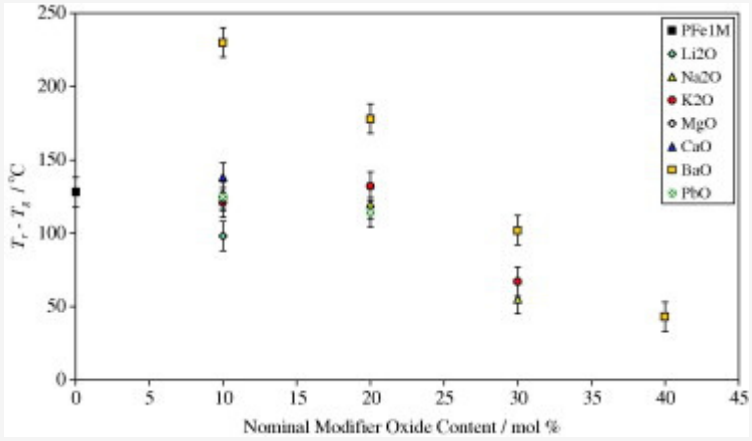

Fig. 3. $T_r–T_g$ as a function of nominal modifier oxide content for $[(1-x)\cdot(0.6P_2O_5–0.4Fe_2O_3)]\cdot xR_yO$ glasses.

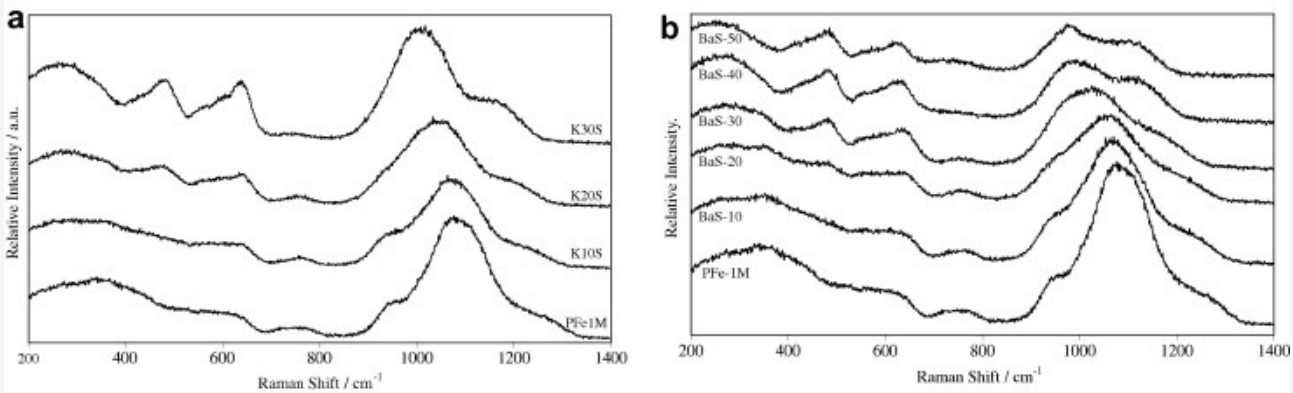

Fig. 4. Raman spectra of (a) $[(1-x)\cdot(0.6P_2O_5–0.4Fe_2O_3)]. xK_2O$ glasses and (b) $[(1-x)\cdot(0.6P_2O_5–0.4Fe_2O_3)]. x$BaO glasses.

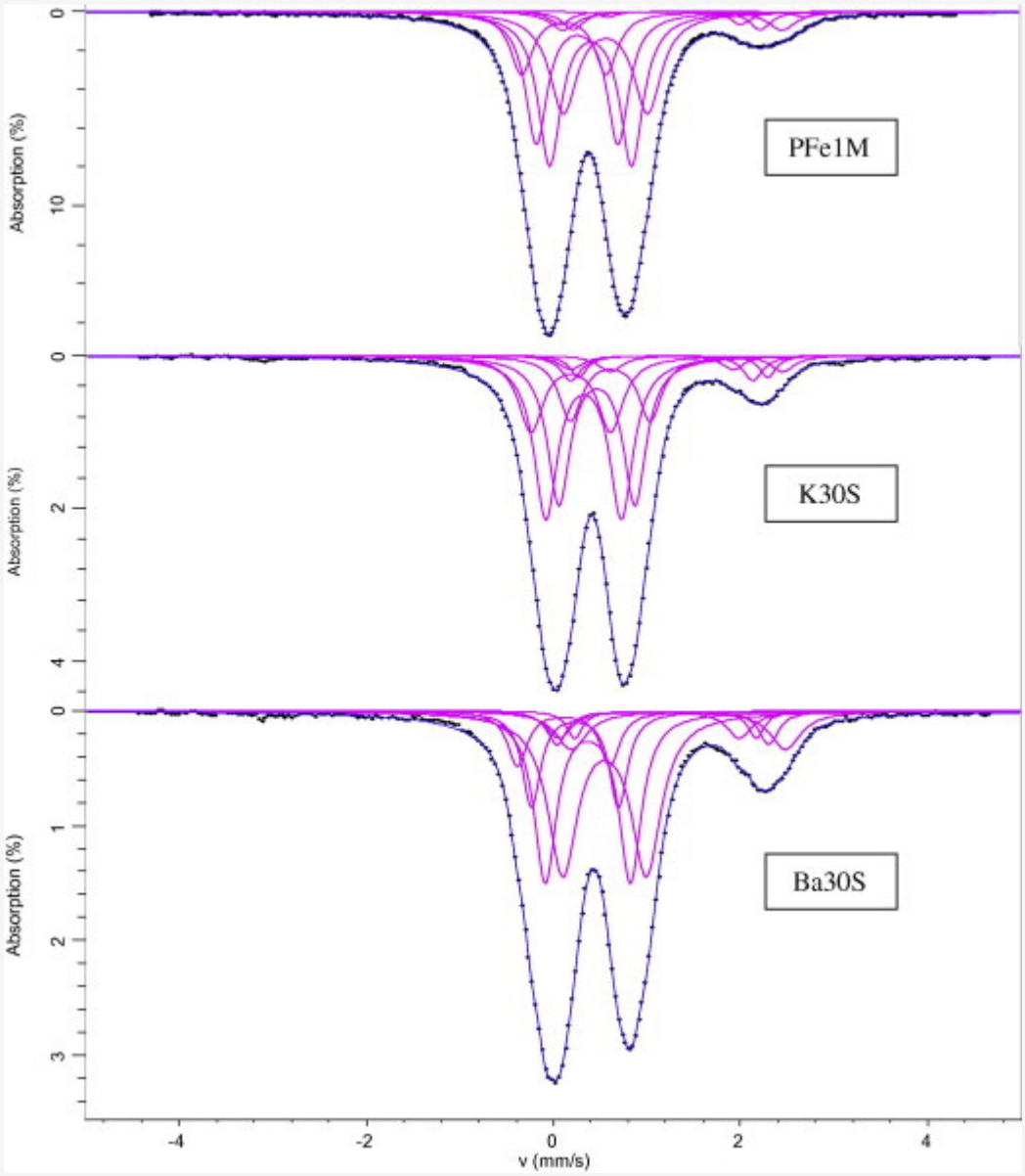

Fig. 5. Selected fitted ^{57}Fe Mössbauer spectra.

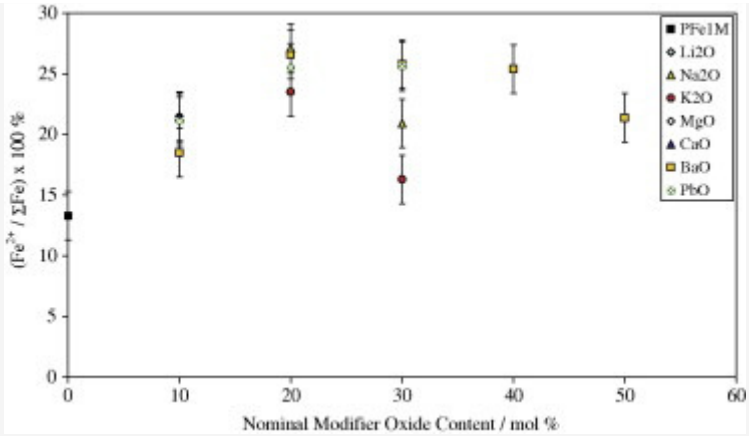

Fig. 6a. Iron redox ratio, $Fe^{2+}/\Sigma Fe$, as a function of nominal modifier oxide content.

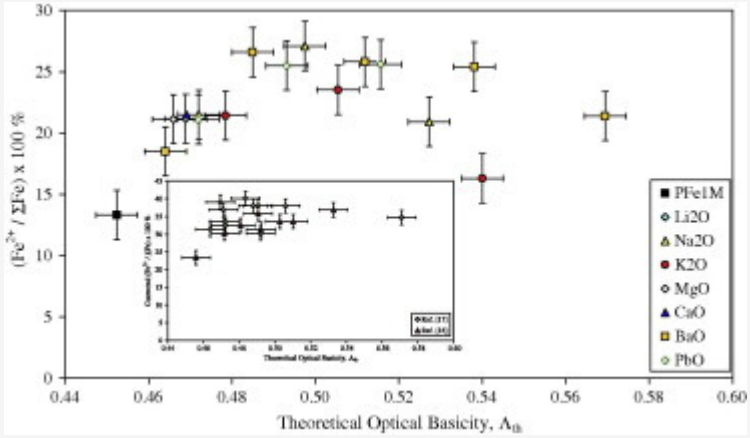

Fig. 6b. Iron redox ratio, $Fe^{2+}/\Sigma Fe$, as a function of theoretical optical basicity calculated from analyzed glass compositions. Embedded graph shows data adapted from Marasinghe et al.[16] and [17].

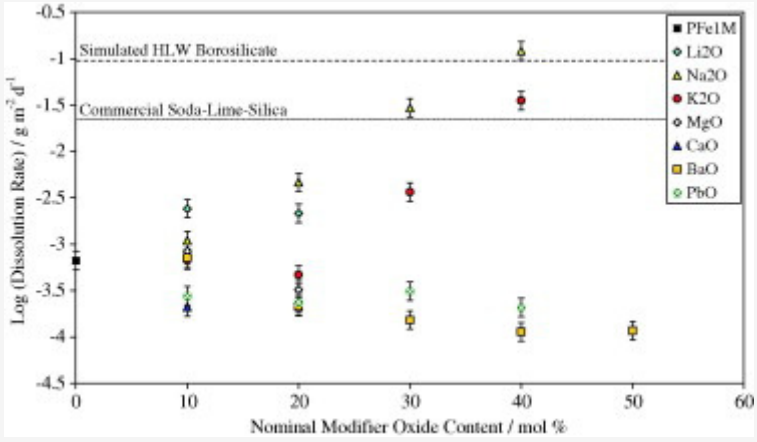

Fig. 7. Aqueous dissolution rate measured by PCT-B vs. nominal modifier oxide content for $[(1-x)\cdot(0.6P_2O_5-0.4Fe_2O_3)]\cdot xR_yO$ glasses.

References

[1] C.M. Jantzen. *J. Non-Cryst. Solids*, **84** (1986), p. 215. **Article** | PDF (582 K) | | View Record in Scopus | | Cited By in Scopus (15)

[2] I.W. Donald, B.L. Metcalfe and R.N.J. Taylor. *J. Mat. Sci.*, **32** (1997), p. 5851. | View Record in Scopus | | **Full Text** via CrossRef | Cited By in Scopus (193)

[3] B.C. Sales and L.A. Boatner, W. Lutze, R.C. Ewing, Editors , *Radioactive Waste Forms for the Future*, North-Holland, Amsterdam (1988) p. 193.

[4] A.P. Mukhamet-Galeyev, L.O. Magazina, K.A. Levin, N.D. Samotoin, A.V. Zotov and B.I. Omelianenko. *Mat. Res. Soc. Symp. Proc.*, **353** (1995), p. 79.

[5] V.V. Kushnikov, Yu.I. Matyunin, T.V. Smelova and A.V. Demin. *Mat. Res. Soc. Symp. Proc.*, **465** (1997), p. 55.

[6] P.A. Bingham and R.J. Hand. *J. Hazard. Mater.*, **B119** (2005), p. 125.

[7] P.A. Bingham, R.J. Hand, S.D. Forder and A. Lavaysierre. *J. Hazard. Mater.*, **B122** (2005), p. 129.

[8] I.W. Donald, B.L. Metcalfe, S.K. Fong, in: Proceedings of the Twentieth International Congress on Glass, Kyoto, Japan, 2004..

[9] P.A. Bingham, R.J. Hand, S.D. Forder, A. Lavaysierre, F. Deloffre, S. Kilcoyne and I. Yasin. *Glass Technol. Eur. J. Glass Sci. Technol. Part B*, **47** (2006), p. 313.

[10] P.A. Bingham, R.J. Hand and S.D. Forder. *Mater. Res. Bull.*, **41** (2006), p. 1622.

[11] Y. Lin, Y. Zhang, W. Huang, K. Lu and Y. Zhao. *J. Non-Cryst. Solids*, **112** (1989), p. 136.

[12] T. Takahashi, T. Inamura, T. Toriyama and H. Iijima. *Nucl. Instrum. Methods Phys. Res. Sect. B*, **76** (1993), p. 103.

[13] P.A. Bingham, S.D. Forder, R.J. Hand and A. Lavaysierre. *Hyperfine Interact.*, **165** (2005), p. 135.

[14] H. Itoh, T. Inamura, H. Wakabayashi, T. Toriyama, H. Iijima, in: Proceedings of the ICAME-95, 1996, p. 445..

[15] X. Yu, D.E. Day, G.J. Long and R.K. Brow. *J. Non-Cryst. Solids*, **215** (1997), p. 21.

[16] G.K. Marasinghe, M. Karabulut, X. Fang, C.S. Ray, D.E. Day, D.L. Caulder, J.J. Bucher, N.M. Edelstein, D.K. Shuh and P.G. Allen.*Ceram. Trans.*, **107** (2000), p. 115.

[17] G.K. Marasinghe, M. Karabulut, C.S. Ray, D.E. Day, P.G. Allen, J.J. Bucher, N.M. Edelstein, D.K. Shuh, Y.S. Badyal, M.L. Saboungi, M. Grimsditch, S.D. Shastri and D. Haeffner. *Ceram. Trans.*, **93** (1999), p. 195.

[18] G.K. Marasinghe, M. Karabulut, C.S. Ray, D.E. Day, C.H. Booth, P.G. Allen and D.K. Shuh. *Ceram. Trans.*, **87** (1998), p. 261.

[19] X. Fang, C.S. Ray, G.K. Marasinghe and D.E. Day. *J. Non-Cryst. Solids*, **263&264** (2000), p. 293.

[20] M. Karabulut, E. Melnik, R. Stefan, G.K. Marasinghe, C.S. Ray, C.R. Kurkjian and D.E. Day. *J. Non-Cryst. Solids*, **288** (2001), p. 8.

[21] A. Mogus-Milankovic, A. Gajovic, A. Santic and D.E. Day. *J. Non-Cryst. Solids*, **289** (2001), p. 204.

[22] Y.M. Moustafa. *J. Phys. D. Appl. Phys.*, **32** (1999), p. 2278.

[23] A. Mogus-Milankovic, K. Furic and D.E. Day. *Mat. Res. Soc. Symp. Proc.*, **663** (2001), p. 153.

[24] M.G. Mesko, D.E. Day and B.C. Bunker. *Waste Manage.*, **20** (2000), p. 271.

[25] M. Karabulut, G.K. Marasinghe, C.S. Ray, D.E. Day, O. Ozturk and G.D. Waddill. *J. Non-Cryst. Solids*, **249** (1999), p. 106.

[26] A.M. Sanad, I. Kashif, M.A. Khaled, S.A. Aly and H. Farouk. *Phys. Chem. Glasses*, **30** (1989), p. 27.

[27] B.L. Metcalfe, S.K. Fong and I.W. Donald. *Glass Technol.*, **46** (2005), p. 130.

[28] A. Mogus-Milankovic, A. Santic, A. Gajovic and D.E. Day. *J. Non-Cryst. Solids*, **325** (2003), p. 76.

[29] M. Hafid, T. Jermoumi, N. Niegisch and M. Mennig. *Mater. Res. Bull.*, **36** (2001), p. 2375.

[30] T. Jermoumi, M. Hafid and N. Toreis. *Phys. Chem. Glasses*, **43** (2002), p. 129.

[31] P. Bergo, S.T. Reis, W.M. Pontuschka, J.M. Prison and C.C. Motta. *J. Non-Cryst. Solids*, **336** (2004), p. 159.

[32] S.T. Reis, M. Karabulut and D.E. Day. *J. Non-Cryst. Solids*, **292** (2001), p. 150.

[33] T. Jermoumi, M. Hafid, N. Niegisch, M. Mennig, A. Sabir and N. Toreis. *Mater. Res. Bull.*, **37** (2002), p. 49.

[34] P.A. Bingham and R.J. Hand. *Mater. Res. Bull.*, **43** (2008), p. 1679.

[35] P.A. Bingham, R.J. Hand, S.D. Forder, A. Lavaysierre, S.H. Kilcoyne and I. Yasin. *Mater. Lett.*, **60** (2006), p. 844.

[36] N.J. Cassingham, P.A. Bingham, R.J. Hand and S.D. Forder. *Glass Technol. Eur. J. Glass Sci. Technol. Part A*, **49** (2008), p. 21.

[37] K.Lagarec, D.G. Rancourt, Recoil: Mössbauer Spectral Analysis Software for Windows, 1998. Available from<http://www.isapps.ca/recoil/.>.

[38] ASTM C1285-02, Standard Test methods for Determining Chemical Durability of Nuclear, Hazardous, and Mixed Waste Glasses: the Product Consistency Test (PCT), ASTM, Conshohocken, USA, 2002..

[39] J.A. Duffy and M.D. Ingram. *J. Non-Cryst. Solids*, **21** (1976), p. 373.

[40] J.A. Duffy. *Geochim. Cosmochim. Acta*, **57** (1993), p. 3961.

[41] A. Dietzel, . *Glastech. Ber.*, **21** (1948), p. 41 81.

[42] J.E. Shelby, An Introduction to Glass Science and Technology, (second Ed.), Royal Society of Chemistry, Cambridge, UK (2005).

[43] M.B. Volf, Mathematical Approach to Glass, Elsevier, Amsterdam (1988).

[44] X. Fang, C.S. Ray, A. Moguš-Milanković and D.E. Day. *J. Non-Cryst. Solids*, **283** (2001), p. 162.

[45] R.K. Brow, R.J. Kirkpatrick and G.L. Turner. *J. Am. Ceram. Soc.*, **76** (1993), p. 919.

[46] B.C. Sales, L.A. Boatner and J.O. Ramey. *J. Non-Cryst. Solids*, **232–234** (1998), p. 107.

[47] B. Tischendorf, J.U. Otaigbe, J.W. Wiench, M. Pruski and B.C. Sales. *J. Non-Cryst. Solids*, **282** (2001), p. 147.

[48] M.W.G. Lockyer, D. Holland, A.P. Howes and R. Dupree. *Solid State Nucl. Magn. Reson.*, **5** (1995), p. 23.

[49] G. Walter, J. Vogel, U. Hoppe and P. Hartmann. *J. Non-Cryst. Solids*, **296** (2001), p. 212.

[50] R.J. Kirkpatrick and R.K. Brow. *Solid State Nucl. Magn. Reson.*, **5** (1995), p. 9.

[51] J. van Wazer, Phosphorus and Its Compounds, vols 1&2, Interscience, New York, USA, 1951..

[52] A. Moguš-Milanković, M. Rajić, A. Drašner and R. Trojko. *Phys. Chem. Glasses*, **39** (1998), p. 70.

[53] A. Moguš-Milanković, A. Šantić, S.T. Reis, K. Furić and D.E. Day. *J. Non-Cryst. Solids*, **342** (2004), p. 97.

[54] I. Ardelean, D. Rusu, C. Andronache and V. Ciobotă. *Mater. Lett.*, **61** (2007), p. 3301.

[55] R.K. Brow, D.R. Tallant, W.L. Warren, A. McIntyre and D.E. Day. *Phys. Chem. Glasses*, **38** (1997), p. 300.

[56] G.K. Marasinghe, M. Karabulut, C.S. Ray, D.E. Day, M.G. Shumsky, W.B. Yelon, C.H. Booth, P.G. Allen and D.K. Shuh. *J. Non-Cryst. Solids*, **222** (1997), p. 144.

[57] C.H. Booth, P.G. Allen, J.J. Bucher, N.M. Edelstein, D.K. Shuh, G.K. Marasinghe, M. Karabulut, C.S. Ray and D.E. Day. *J. Mater. Res.*, **14** (1999), p. 2628.

[58] M. Karabulut, G.K. Marasinghe, C.S. Ray, D.E. Day, G.D. Waddill, P.G. Allen, C.H. Booth, J.J. Bucher, D.L. Caulder, D.K. Shuh, M. Grimsditch and M.L. Saboungi. *J. Mater. Res.*, **15** (2000), p. 1972.

[59] M. Karabulut, G.K. Marasinghe, C.S. Ray, G.D. Waddill, D.E. Day, Y.S. Badyal, M.L. Saboungi, S. Shastri and D. Haeffner. *J. Appl. Phys.*, **87** (2000), p. 2185.

[60] U. Hoppe, M. Karabulut, E. Metwalli, R.K. Brow and P. Jóvári. *J. Phys. Condens. Matter*, **15** (2003), p. 6143.

[61] A.C. Wright, R.N. Sinclair, J.L. Shaw, R. Haworth, G.K. Marasinghe and D.E. Day. *Phys. Chem. Glasses Eur. J. Glass Sci. Technol. Part B*, **49** (2008), p. 1.

[62] R.G.C. Beerkens and K. Kahl. *Phys. Chem. Glasses*, **43** (2002), p. 189.

[63] J.A. Duffy. *J. Non-Cryst. Solids*, **196** (1996), p. 45.

[64] R.J. Edwards, A. Paul and R.W. Douglas. *Phys. Chem. Glasses*, **13** (1972), p. 131.

[65] G. Jeddeloh. *Phys. Chem. Glasses*, **25** (1984), p. 163.

[66] P.A. Bingham, J.M. Parker, T. Searle, J.M. Williams and I. Smith. *C.R. Chim.*, **5** (2002), p. 787.

[67] H.D. Schreiber, B.K. Kochanowski, C.W. Schreiber, A.B. Morgan, M.T. Coolbaugh and T.G. Dunlap. *J. Non-Cryst. Solids*, **177** (1994), p. 340.

[68] C. Mercier, G. Palavit, L. Montagne and C. Follet-Houttemane. *C.R. Chim.*, **5** (2002), p. 693.

[69] J. Koo, B.-S. Bae and H.-K. Na. *J. Non-Cryst. Solids*, **212** (1997), p. 173.

[70] B.-S. Bae and M.C. Weinberg. *J. Am. Ceram. Soc.*, **74** (1991), p. 3039.

[71] M.M. Morsi, E.E.S. Metwalli and A.A. Mohammed. *Phys. Chem. Glasses*, **40** (1999), p. 314.

[72] L. Bih, L. Abbas, A. Nadiri, H. Khemakhem and B. Elouadi. *J. Mol. Struct.*, **872** (2008), p. 1.

[73] A. Paul and R.W. Douglas. *Phys. Chem. Glasses*, **6** (1965), p. 207.

[74] M.D. Dyar. *Am. Mineral.*, **70** (1985), p. 304.

[75] S. Sekhon and R. Kamal. *Phys. Chem. Glasses*, **29** (1988), p. 157. | View Record in Scopus | | Cited By in Scopus (4)

[76] T. Nishida. *J. Non-Cryst. Solids*, **177** (1994), p. 257. **Article** | PDF (874 K) | | View Record in Scopus | | Cited By in Scopus (32)

[77] M.I. Ojovan and W.E. Lee, An Introduction to Nuclear Waste Immobilisation, Elsevier, Amsterdam (2005).

[78] B.C. Bunker, G.W. Arnold and J.A. Wilder. *J. Non-Cryst. Solids*, **64** (1984), p. 291. **Article** | PDF (1134 K) | | View Record in Scopus | | Cited By in Scopus (156)

[79] Y.B. Peng and D.E. Day. *Glass Technol.*, **32** (1991), p. 166. | View Record in Scopus | | Cited By in Scopus (107)

[80] T. Minami and J.D. Mackenzie. *J. Am. Ceram. Soc.*, **60** (1977), p. 232. | View Record in Scopus | | Cited By in Scopus (32)

[81] E. Metwalli and R.K. Brow. *J. Non-Cryst. Solids*, **289** (2001), p. 113. **Article** | PDF (386 K) | | View Record in Scopus | | Cited By in Scopus (40)

[82] P.Y. Shih and H.M. Shiu. *Mater. Chem. Phys.*, **106** (2007), p. 222. **Article** | PDF (493 K) | | View Record in Scopus | | Cited By in Scopus (6)

[83] J.J. Shyu and C.H. Yeh. *J. Mater. Sci.*, **42** (2007), p. 4772. | View Record in Scopus | | **Full Text** via CrossRef | Cited By in Scopus (10)

[84] B.H. Jung, D.N. Kim and H.S. Kim. *J. Non-Cryst. Solids*, **351** (2005), p. 3356. **Article** | PDF (206 K) | | View Record in Scopus | | Cited By in Scopus (11)

[85] L. Kahl. *Adv. Ceram.*, **20** (1986), p. 141.

[86] W.G. Ramsey, N.E. Bibler, T.F. Meaker, Compositions and Durabilities of Glasses for Immobilization of Plutonium and Uranium (IV), WSRC-MS-94–0550, 1995 <http://www.osti.gov/bridge/servlets/purl/63953-Dcglhu/webviewable/.>.